

# First Evidence of Nanodiamond Clusters Formation in Shungite in Connection With Seismogenic Dynamic Shear

Corresponding Member of the RAS Yu. A. Morozov<sup>a,\*</sup>, A. S. Aronin<sup>b</sup>, O. I. Barkalov<sup>b</sup>,  
K. A. Gavrilicheva<sup>b</sup>, V. M. Kozlovsky<sup>c,d</sup>, and M. A. Matveev<sup>a</sup>

<sup>a</sup>*Schmidt Institute of Physics of the Earth, Russian Academy of Sciences, Moscow, 123995 Russia*

<sup>b</sup>*Institute of Solid State Physics, Russian Academy of Sciences, Chernogolovka, Moscow oblast, 142432 Russia*

<sup>c</sup>*Institute of Mineralogy, Geochemistry, and Crystallochemistry of Rare Elements, Moscow, 121357 Russia*

<sup>d</sup>*Institute of Geology of Ore Deposits, Petrography, Mineralogy, and Geochemistry, Russian Academy of Sciences, Moscow, 119017 Russia*

\*e-mail: frost@ifz.ru

Received March 11, 2025; revised April 1, 2025; accepted April 7, 2025

**Abstract**—The first evidence for the natural transformation of originally amorphous carbon into graphite and diamond nanoclusters under the influence of high-speed dynamic shearing and the associated frictional heating of the carbonaceous substratum is presented in the example of Karelian shungites and seismogenic slickensides identified in them. Approximate estimates of the *PT* parameters of these structural, material, and phase transformations are given, and their position on the phase diagram of carbon is noted.

**Keywords:** shungite, glassy carbon, graphite, nanodiamond, seismogenic shears, slickensides

**DOI:** 10.1134/S1028334X2560639X

## INTRODUCTION

The study of the products of structural and material transformations of rocks in faults, in areas of localized deformations, and in zones of other dynamic dislocations, including seismogenic ones, is an important area of research in Earth sciences, whether for solving the problems of tectonics and geodynamics, petrology, and geochemistry, or geomechanics and seismology. It is within the framework of this problem field that the issues are being posed and solved for the structural and textural reorganization of rock matrix and the corresponding changes in its petrophysical properties; mechanisms of mineral matter redistribution; differential mobility of chemical elements under the influence of stress; and thermodynamic parameters of such obviously nonlinear processes. No less significant is their study to assess the conditions of mechanical instability in fault dislocations responsible for seismicity manifestations in the Earth's crust, the specifics of preparation for and initiation of rock destruction in earthquake source zones, and the structural and phase transformations occurring there that significantly affect the seismic mobility regime [1, 2]. The new materials and results presented here, concerning specific transformation of the natural carbon matter of shungite varieties of rocks exposed to high-velocity shearing of the presumed seismogenic character, fit exactly into this direction of research. The study of numerous slickensides found in them and the specific

features of the structural transformations of carbon material that occurred in this process led to the identification of several allotropic modifications of carbon, including its nanodiamond clusters, which have been detected here in the natural setting for the first time.

## FACTUAL MATERIAL

The study of carbon matter transformation in zones of dynamic shearing was started earlier using the example of carbonaceous carbonate rocks, where syn-deformation changes in carbon isotope composition were evaluated [3], and Karelian shungites, where mainly structural and material changes in the substratum were considered [4]. Widespread in the Onega Paleoproterozoic structure of the Karelian craton, shungites have drawn attention by the abundance of dislocations of presumably seismogenic origin in the form of pronounced slickenside planes, often associated with zones of brittle brecciation of the shungite matrix (Fig. 1).

Apart from carbon matter, the volume content of which varies from 10–20 to 45–60% and more in the identified varieties, shungites contain quartz, potassium feldspar, flaky silicates (chlorite, muscovite, phengite, minerals of the epidote group, biotite), calcite, dolomite, and a certain amount of accessory minerals (pyrite, chalcopyrite, sphalerite, galena, rutile, apatite, zircon, calcite, etc.). They underwent

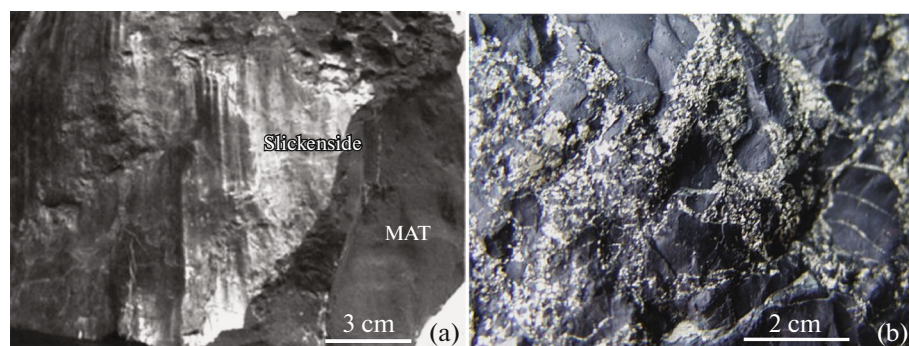


**Fig. 1.** Samples of shungite with elements of seismogenic shearing. (a) Slickenside surface on the original shungite matrix (MAT); (b) structures of shungite brecciation with fragments cemented by quartz-sulfide material.

regional metamorphism within the greenschist facies of metamorphism, the parameters of which are estimated by temperature (by the calcite-dolomite thermometer) in the range of 350–430°C, and by pressure (by the phengite barometer) of about 5 kbar [5]. As for the carbon matter proper, its origin is usually attributed to the transformation during metamorphism of organosiliceous sedimentary material (sapropelite), where it reached the metaanthracite stage of carbonization. At the same time, some textural, chemical, and isotopic indications of fluidogenic origin of carbon, as well as its fluid dynamic redistribution in the rock substratum, have been found in certain places [6].

There is still no definitive answer as to what allotropic variety of carbon the shungite substance belongs to. According to some researchers, it is an amorphous modification [7], while others believe that “shungite carbon is not just amorphous carbon but is a mixture of various carbon allotropes whose small lattices are connected by amorphous carbon” [8]. In addition, it is assigned either to fullerene-like varieties [9] or to natural glassy carbon [10], in which graphene and fullerene-like motifs are mixed. We have studied analytically two structural varieties of shungite rock from the mined Zazhogino and Maksovo deposits: the original massive matrix (MAT) and its finely textured modification in the slickenside film with a “metallic” luster and linearly striated structure (Fig. 1a).

## METHODOLOGY

The study of the microstructure of shungite rocks and determination of their mineral phase composition was carried out using a set of instrumental and analytical methods. The total and elemental compositions of the original matrix and slickenside film of the shungite sample were examined at the Frumkin Institute of Physical Chemistry and Electrochemistry of the Russian Academy of Sciences by X-ray electron probe analysis. The studies were carried out on a scanning electron microscope JSM-U3 by JEOL (Japan) with a

GETAC attachment for digital scanning and energy dispersive X-ray spectrometer WinEDS with a resolution of 200 Å.

The results of transmission electron microscopy of shungites were obtained at the Osipian Institute of Solid State Physics of the Russian Academy of Sciences (ISSP RAS, Chernogolovka) using a JEM100CX11 microscope (Jeol, Japan) at an accelerating voltage of 100 kV. The shungite and slickenside samples were also studied by Raman spectrometry (RS) using a Princeton Instruments HRS 500 spectrometer with a CCD detector cooled by liquid nitrogen on a diffraction grating with a groove density of 1200 grooves/mm at room temperature. A 532.179 nm KLM-532/SLN-100 DPSS laser (FTI-Optronik, St. Petersburg; the emission power on the sample was 5 mW) was used for excitation. The optical system was operated in the backscatter geometry, and a 20x Plan Apo Mitutoyo 20x lens was used to focus the laser light and collect the light scattered by the sample, giving a focal spot size on the sample of approximately 3 μm. A holographic Tydex Notch-6 filter (Tydex, St. Petersburg) was used to discriminate the excitation line, thereby capturing Raman spectra from a frequency of 200 cm<sup>-1</sup>. The spectral resolution in this range was about 1 cm<sup>-1</sup>. The measurement accuracy of ±1 cm<sup>-1</sup> was achieved by calibrating the spectrometer using the Ne emission lines.

Additional study of Raman spectra in the visible light range was carried out at the Nesmeyanov Institute of Organoelement Compounds, RAS, on a Horiba-Jobin-Yvon LabRAM-300 spectrometer, with the excitation laser line of 632 nm at 3 mW. In addition, Raman spectra were obtained at the IMGRE laboratory center as part of the refinement of the technique for analyzing carbon materials on a Confotec NR-500 spectrometer. A semiconductor laser with an excitation line of 473 nm and a wattage of 63.7 mW was used. To minimize sample degradation, a 10-fold neutral filter was used to reduce the excitation laser power. To detail the spectrum in the 870–1800 cm<sup>-1</sup> region, a diffraction grating was used with an increased number

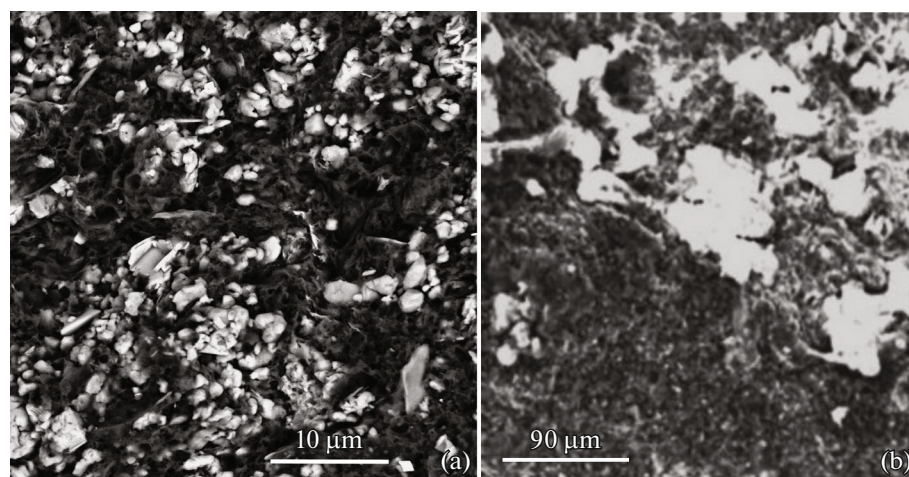


**Fig. 2.** BSE images of the structure of the massive shungite matrix MAT (a). The substratum of the shungite matter is displayed in dark tones; grains of quartz, potassium feldspar and micas are light. Redeposited quartz aggregates (light) in the shungite substratum (b).

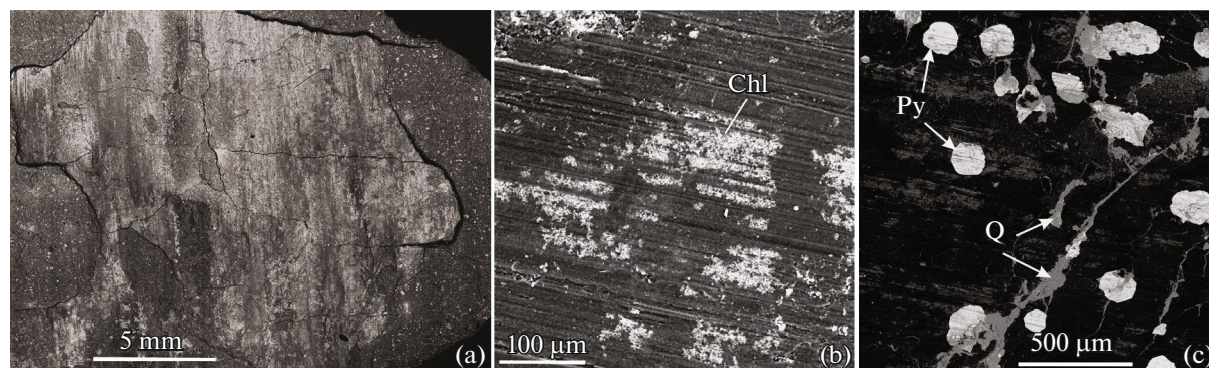


**Fig. 3.** BSE images of the slickenside film against the background of original shungite (a), linear striation on the slickenside surface (b), and its superposition over pyrite crystals (c). Q – quartz, Py – pyrite, Chl – chlorite.

of grooves, 1800 lines/mm, and a 50x/0.55 lens. The laser beam focusing diameter on the sample was 1–1.5 μm; the spectral resolution was 1 cm<sup>-1</sup>. The spectrum was calibrated on the excitation laser line with control along the metallic Si line.

The shungite sample on its two surfaces (MAT and slickenside) was also examined at the Institute of Solid State Physics, RAS, by X-ray diffraction on a Siemens D500 diffractometer (Siemens, FRG) in CoK<sub>α</sub> radiation.

### ANALYTICAL RESULTS

The study of the nature of the structure, bulk and elemental compositions of the shungite matrix and slickenside film by electron probe X-ray spectroscopy and scanning microscopy showed that the massive original substratum (MAT) is formed mainly by grains of quartz, potassium feldspar, and other aforementioned silicate minerals, which are surrounded by the

shungite matter (Fig. 2a). Quartz is also present in separate areas and in the clearly redeposited form as cementing material of breccias (see Fig. 1b), in larger aggregates of irregular shapes (Fig. 2b), and in vein forms (Fig. 3c). The slickenside film at the microlevel has a completely different, thin-plate structure (Fig. 3a), losing its original granular appearance and acquiring a linearly striated structure (Fig. 3b), which is superimposed, among other things, on pyrite crystals in the shungite matrix (Fig. 3c).

Along with changes in the structure of the shungite substratum in the zone of dynamic dislocation, there were significant changes in its elemental and mineral phase composition (Table 1).

Above all, we note the directly opposite trends in carbon and silicon concentrations: in the slickenside film, the content of the former grows significantly, while the latter clearly decreases compared to the initial composition of shungite (Fig. 4a). This can be attributed to the ease with which quartz transitions

**Table 1.** Elemental composition of MAT substratum and slickenside obtained using EPMA

Element	Variety			
	MAT		slickenside	
	at %	wt %	at %	wt %
C	47.7	38.04	72.35	60.96
O	34.85	37.90	19.04	21.20
Mg	0.22	0.23	0.18	0.31
Al	0.80	1.48	1.26	2.37
Si	13.64	21.51	4.31	8.43
S	0.16	0.10	0.66	1.47
K	0.23	0.59	0.47	1.27
Fe	0.18	0.15	0.90	3.50
P	—	—	0.13	0.28
Zn	0.04	—	—	—
Cu	0.09	—	—	—
Ti	1.99	—	—	—
Cl	0.06	—	—	—
Total	100	100	100	100

into orthosilicic acid gel during seismic dislocations [1, 2] and to the destruction of skeleton silicates replaced by layered minerals such as hydromica and chlorite. The latter two, as it can be seen (see Figs. 3b, 3c), immediately settle in the zone of movement into patchy accumulations of fine-grained unoriented aggregate, while quartz is redeposited in vein-injected forms in adjacent areas of the damaged substratum (see Figs. 2b and 3c). The general enrichment of the slickenside film with carbon (up to 60–77 wt % with the initial content of 26–34 wt % in the MAT variety) is probably associated in this case with its relatively lower mobility, although there are also indications of its fluid dynamic redistribution, as already noted [6]. This is probably the reason for the significant unevenness in its concentration (as well as that of other elements) in the displacement zone, differing by several times from one place to another (Figs. 4b–4d).

Such high mobility of elements can be assumed to be related to tribochemical transformations [1] and

frictional heating of the substratum in the zone of dynamic displacement to temperatures of 1450–1650°C, if one is to judge by comparing the Raman spectra of shungite in slickenside with spectra of different grades of glassy carbon annealed at different temperatures [4].

Along with changes in the mineral phase and bulk chemical composition of shungite in the slickenside film, significant structural transformations of the carbon material occur as well. Transmission microscopy allowed to visualize bright clusters of graphite and nanodiamonds in the carbon material of the slickenside film, surrounding areas of amorphous carbon (Fig. 5). The size of individual particles in these formations is estimated in the range of 5–10 nm. Microdiffraction patterns of such particles confirm the presence of both graphite and diamond (Fig. 6), and the uneven distribution of the intensity of ring reflections indicates the manifestation of an ordered texture in the film, which is evident from its flake-like composition in the bright-field image (Fig. 7). The processing results for electron diffraction patterns of both allotropic modifications given in Table 2 show a good correspondence between the values of the obtained interplanar distances ( $d$ , experiment) in their crystal lattices and similar theoretical data ( $d$ , theoretical) for diamond and graphite.

The substratum in the studied samples was also examined by Raman spectroscopy in different measurement modes in several areas: on arbitrary external surfaces of the massive shungite variety (MAT), on its section 1 mm below the slickenside (SECTION), and directly on the slickenside film itself. This allowed us to partially verify the noted changes in the structural state of the carbon material.

The MAT variety spectra obtained at different values of the laser excitation line (Fig. 8) proved to be quite typical of disordered carbon modifications with a mixed type of hybridization, namely, with first-order D (1331  $\text{cm}^{-1}$ ), G (1598  $\text{cm}^{-1}$ ), and second-order 2D (2700  $\text{cm}^{-1}$ ) lines [11]. This may correspond to a combination of graphene fragments with  $\text{sp}^2$  bonds (G band) and diamond-like  $\text{sp}^3$  bonds (D band), characteristic of amorphous carbon and carbon material with a high degree of topological defects and dislocations in the initially ordered structure. Note here the

**Table 2.** Table of interplanar distances based on the processed electron diffraction patterns for two slickenside areas; normalized to plane 111

Electron diffraction pattern 32314			Electron diffraction pattern 32324		
$d$ , exper. Å	$d$ , theor. Å	plane $hkl$	$d$ , exper. Å	$d$ , theor. Å	plane $hkl$
2.06	2.06	(111) diamond	3.39	3.38	(002) graphite
1.22	1.25	(220) diamond	2.06	2.06	(111) diamond
1.05	1.07	(311) diamond	1.22	1.25	(220) diamond
			1.05	1.07	(311) diamond

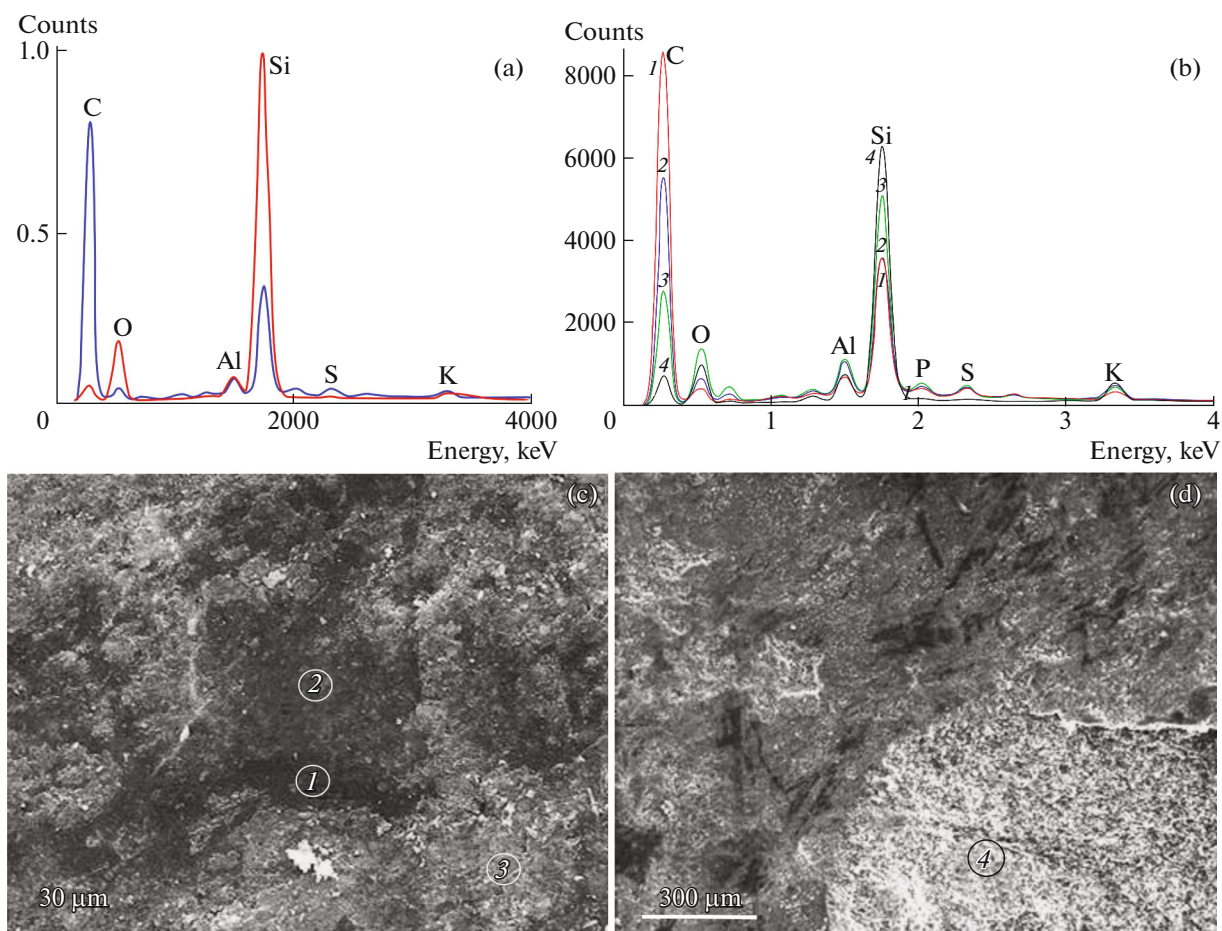


**Fig. 4.** Comparison of spectra of elemental compositions (a) of the original shungite matrix MAT (red curve) and slickenside film (blue). The vertical axis shows elements contents in accepted units. Spectra of the elemental composition of the slickenside film in some areas (b) with a varying degree of the substratum's carbon material filling in the domains indicated by numbers 1–4 in (c) and (d).

variability of the  $I_D/I_G$  disordering index in the carbon structure of the original shungite from one place to another (Fig. 8a), as well as the very high intensity of the D band, indicating the nanocluster state of the carbon material, with a linear particle size of up to 8–10 nm [11]. Moreover, a weak leg (T line) is also observed in the low-frequency part of the D band (Fig. 8b), reflecting, as it is believed, the curvature of graphene layers and the manifestation of  $sp^3$  bonds [11]. The observed parameters are close to those in glassy carbon, although they are somewhat shifted towards the high-frequency region. The presence of additional lines in the frequency range up to  $1000\text{ cm}^{-1}$  (Fig. 8b) is obviously associated with impurity minerals, including quartz (bands 128, 207, and  $466\text{ cm}^{-1}$ ), while the appearance of a noticeable arm on the high-frequency side of the quartz band ( $500\text{--}510\text{ cm}^{-1}$ ), as well as in the  $1400\text{--}1500\text{ cm}^{-1}$  region, may indicate the presence of amorphous carbon [11].

A comparison of the spectra of massive shungite (MAT) and in the slickenside film itself (Fig. 8b) cap-

tures noticeable variations in the ratio of the intensities of the D and G bands, as well as in their positions and configurations [4]. We see that in slickenside the half-width of the D line lies within  $65\text{--}67\text{ cm}^{-1}$  at a frequency of  $1333\text{ cm}^{-1}$ ; the same line in the MAT variety spectra has different parameters: half-width is  $55\text{--}57\text{ cm}^{-1}$  and frequency is  $1331\text{ cm}^{-1}$  (the values given are averaged over the array of measurements). This broadening of the D line indicates an increase in disorder in the carbon structure, which, apparently, is due to an increase in the degree of matrix disturbance during deformation.

An important and pronounced feature of the structural transformations is also the indisputable fact of the directional shift of the G band from  $1587\text{ cm}^{-1}$  towards higher frequency up to  $1595\text{ cm}^{-1}$  in the consecutive series MAT-SECTION-slickenside (Figs. 9a–9c), which may be associated with the above mentioned (see Figs. 5, 6) formation of nanocrystalline graphite in the slickenside film [12], as well as with the effect of dynamic pressure [13].

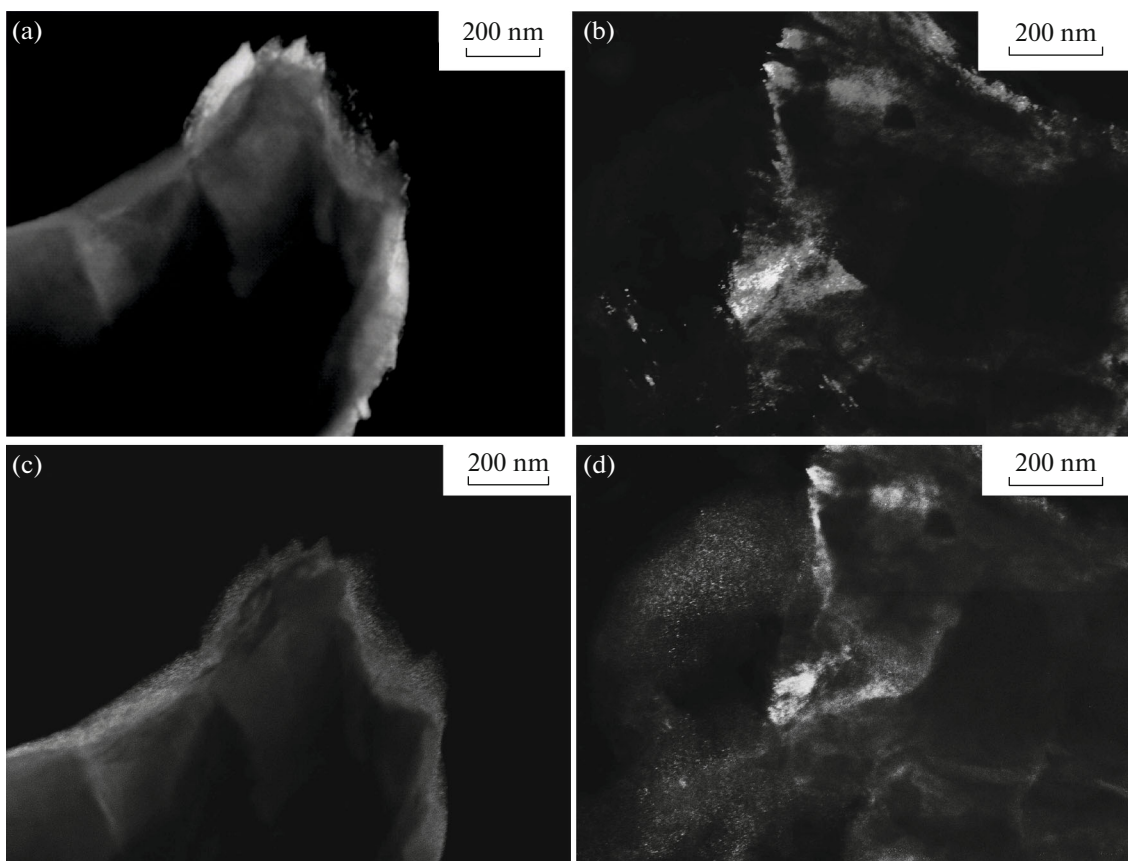


**Fig. 5.** Dark-fields images of slickenside film fragments in reflections of graphite (a and b) and diamond (c and d); bright spots are particles of graphite and diamond in the respective reflections.

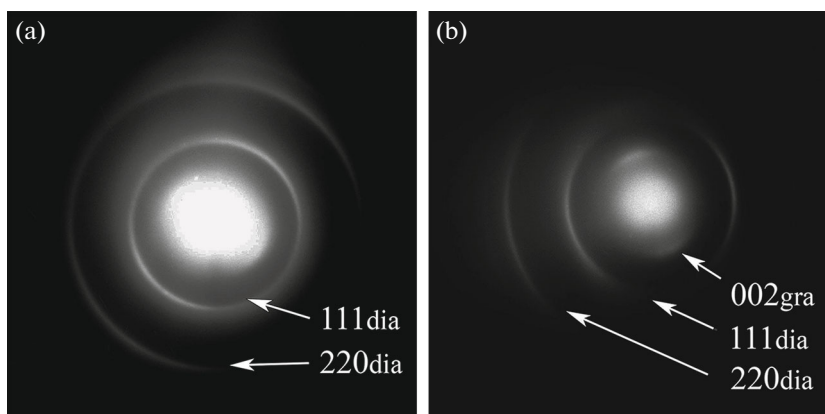


**Fig. 6.** Microdiffraction images of two areas of slickenside film indicating the presence of diamond (a) and of diamond with graphite (b).

As for the nanodiamond phase in slickenside revealed by transmission microscopy, its characteristic spectral mark in the form of a  $1332\text{ cm}^{-1}$  band overlaps with an intensely pronounced D band, the formation of which is generally dominated by small-sized crystallites of different allotropic modifications [11]. However, the use of a 473 nm laser excitation line, whereby

the contribution of background luminescence to the spectrum is much lower compared to excitation by 532 and 632 nm lasers, allowed us to make some interesting observations. The spectra were measured on the slickenside surface of shungite complicated by a network of parallel striations and thin slid striae mentioned above (see Fig. 3) (Fig. 9d). In focusing the

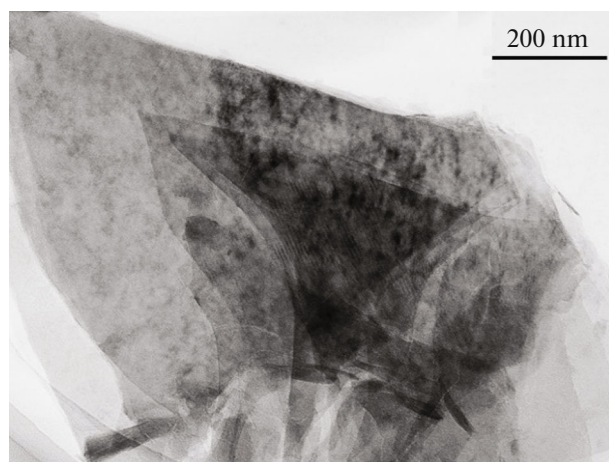


**Fig. 7.** Bright-field image of a slickenside film fragment with elements of ordered crystalline and flaky structure.

laser beam between the striae, the Raman spectra showed peaks at  $1362\text{ cm}^{-1}$  and  $1593\text{ cm}^{-1}$ , uncomplicated by additional lines (Fig. 9e). However, if the laser beam was focused directly into the striae, we clearly observed the appearance of an additional mode of  $1255\text{ cm}^{-1}$  on the low-frequency side of the D peak and an additional mode of  $1525\text{ cm}^{-1}$  on the low-frequency side of the G peak (Fig. 9f). According to [14], these modes are classified as F bands and correspond to the fullerene-like allotrope, an amorphous carbon with a high proportion of  $\text{sp}^3$ -hybridization. In addition, on the low-frequency side of the D peak, a very low-intensity excitation in the region of  $1291\text{ cm}^{-1}$  is detected in the two spectra. After smoothing the background fluctuations and deconvolution of the spectrum using the Gaussian method (inset in Fig. 9f), this

small perturbation can be seen more clearly. We assume that this perturbation corresponds to the spectral line of nanocrystalline diamond. Relative to  $^{12}\text{C}$ -based crystalline diamond, with a characteristic spectral line at  $1332\text{ cm}^{-1}$ , the observed line is shifted to a lower frequency region by  $41\text{ cm}^{-1}$ . Such a shift of the spectral line in nanodiamonds occurs regularly and can be caused by a number of reasons: (1) the transition from macrocrystalline individuals to nanoscale (about  $5\text{ nm}$ ) crystals initiates a shift of the spectral line into the “blue” region by  $16\text{ cm}^{-1}$  [15]; (2) the formation of nanodiamonds in a thermally affected glassy carbon shell leads to a shift of the spectral line due to heating from  $1332\text{ cm}^{-1}$  to  $1321\text{--}1322\text{ cm}^{-1}$ , i.e.,  $\approx 10\text{ cm}^{-1}$  [16]; (3) an increasing fraction of  $^{13}\text{C}$  leads to a shift of the spectral line by  $\approx 52\text{ cm}^{-1}$  from  $1332$  to  $1280\text{ cm}^{-1}$  [17]. With regard to the latter circumstance, it is appropriate to mention here that dynamic shearing promotes fractionation of carbon isotopes and enrichment of the displacement zone with  $^{13}\text{C}$  isotope [3]. Note that not all striae contain nanodiamond peaks. Dominant are the striae in which only F peaks are observed.

Looking at some additional features of the Raman spectra of the slickenside film material, we should also note the almost complete removal of impurity mineral phases, including quartz, which resulted in the disappearance of a series of bands in the frequency range up to  $1000\text{ cm}^{-1}$  (Fig. 8b), observed in the original MAT shungite.

The use of X-ray microdiffraction (XRD) in the analysis of SECTION and slickenside matrixes confirmed the above-mentioned trends of change in their compositions and structure relative to the initial MAT variety (see Table 1), manifested in their successive

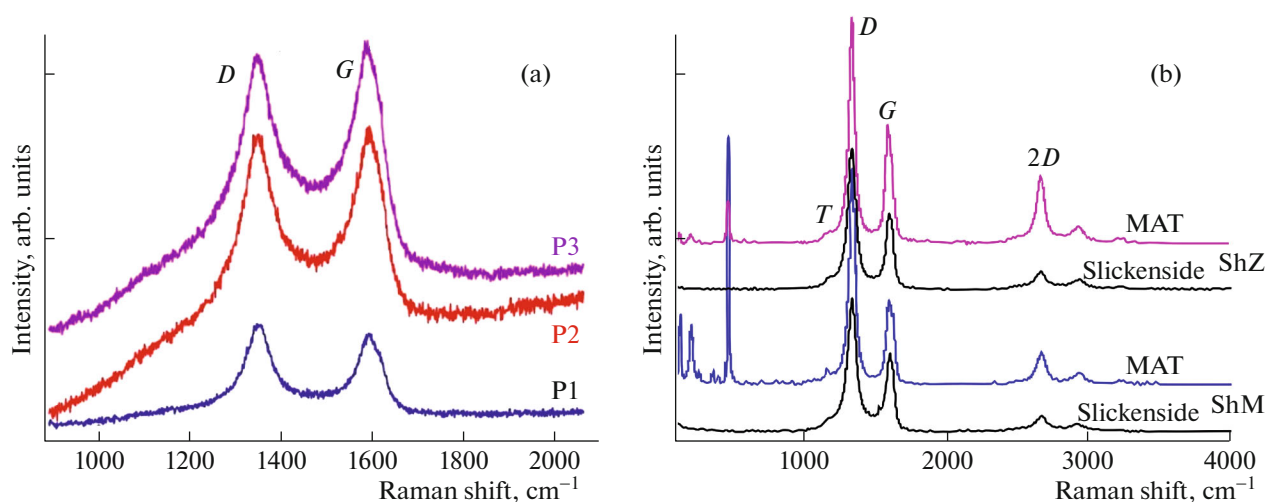


**Fig. 8.** Raman spectra of the original shungite MAT and slickenside over shungite: a MAT sample (a) from the Maksovo deposit (P1–P3 – spectra at different measurement points); spectra of MAT and slickenside varieties (b) from the Zazhogino (ShZ) and Maksovo (ShM) deposits. Spectra (a) were obtained at the  $532\text{ nm}$  excitation line of the laser, and spectra (b) at  $632\text{ nm}$  line.

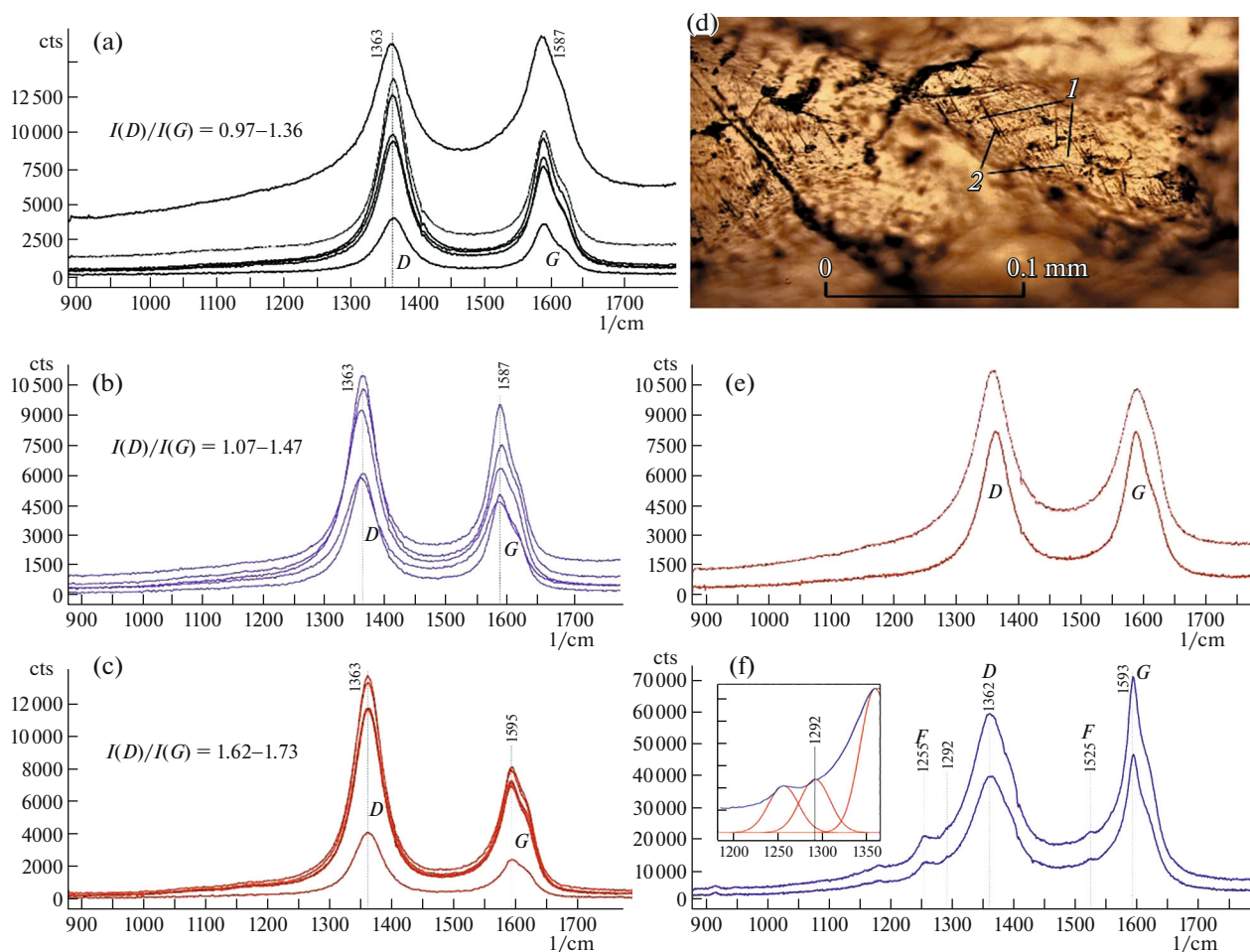


**Fig. 9.** Raman spectra (473 nm laser) of shungite varieties from the Maksovo deposit: MAT (a), SECTION (b), slickenside (c); photograph of the slickenside surface with slid striae (d); the numbers indicate the laser focus points: (1) between striae, (2) in convex striae; Raman spectra between striae (e); Raman spectra in striae (f). The inset in (f) is a spectrum fragment after background fluctuation smoothing and Gaussian deconvolution marking the nanodiamond peak with a maximum at  $1292\text{ cm}^{-1}$ .

enrichment in carbon and the corresponding depletion in quartz and other silicates (Table 3). The same applies to the variability of the structural state of the dominant mineral phases of the shungite substratum when approaching the zone of shearing, registered, in particular, by the increasing manifestation of planar crystalline graphite phases with the dominance of the 002 diffraction line (Fig. 10). Furthermore, the apparent strengthening of peak intensities may indicate both an increase in the degree of graphitization and a growth in the crystallite size, as established experimentally during thermal treatment of amorphous carbon [18], which in our case was caused by frictional heating of the substratum in the zone of shearing.

## DISCUSSION AND CONCLUSIONS

Summarizing the above analytical results on the transformation of carbon matter of shungites in the zone of seismogenic dynamic shearing, we should

emphasize the undisputed influence on the transition of initially amorphous carbon into graphite and diamond nanoclusters of the factors of temperature effect on the substratum, in the form of its frictional heating, and the dynamic effect of high-velocity shear on phase changes, which is in good agreement with experimental data [16]. In addition to the very fact of the appearance of these newly formed carbon allotropes in the slickenside film as detected by transmission microscopy (see Fig. 5), their presence is recorded by Raman spectroscopy and X-ray microdiffraction. In the Raman spectra, the effect of dynamic pressure and the appearance of graphite nanoclusters (see Fig. 9) were expressed in the directional shift toward higher frequencies of the G band along the transition in the MAT-SECTION-slickenside series. The decrease in the 2D band intensity in the slickenside spectra (see Fig. 8b), which is usually associated with the number of graphene layers in the matrix [11], obviously indicates the corresponding growth of “diamond”  $\text{sp}^3$

bonds there. The question of the sequence of formation of graphite and nanodiamond phases (diamonds on graphite or vice versa) remains open, since the presence of  $sp^2$ – $sp^3$  bonds in the initial structure of shungite can be a favorable prerequisite for the formation of both diamond nanoclusters and graphite crystallites. Frictional thermal heating in the plane of displacement may favor the preferential formation of graphene layers, whereas their subsequent deformation may lead to an increased role of diamond-forming  $sp^3$  bonds. The latter option is quite plausible taking into account the localization of nanodiamond clusters in the marginal parts of domains with a graphite structure (see Fig. 5).

In view of the above, and taking into account the polyvariance of scenarios, we can tentatively assume a three-stage pattern in the evolution of carbon matter in slickenside: (1) at the beginning of the process, at the stage of compression, the amorphous carbon is ordered with an increasing share of  $sp^2$  graphite clusters; (2) at the stage of decompression, when mechanical stresses are released, shear fractures appeared, near which  $sp^2$  clusters were deformed to produce fullerene-like domains with a high share of  $sp^3$  hybridization; (3) further ordering of the resulting structure led to the formation of areas enriched in nanocrystalline diamond in some microshears or their fragments.

Turning to the genetic conditions of diamond formation, a detailed review of which is presented in [19], it is important to note an unusually wide range of identified conditions and mechanisms of their genesis, recorded in the  $PT$  coordinates of the carbon phase diagram (Fig. 11). Without referring to all known theoretical and experimental scenarios for the transformation of amorphous carbon into graphite and diamonds, we will only mention those that are closest to our natural variant. First of all, we should note the

**Table 3.** Estimates of compositions of SECTION and slickenside varieties using X-ray microdiffraction

Element	Variety			
	SECTION		slickenside	
	at %	wt %	at %	wt %
C	60.86	71.26	69.03	76.92
O	26.70	23.47	23.67	19.80
Mg	0.36	0.21	0.92	0.46
Al	1.21	0.63	5.07	2.42
Si	6.00	3.00	0.18	0.07
S	0.79	0.35	0.17	0.06
K	0.50	0.18	0.34	0.12
Fe	3.59	0.91	69.03	76.92
Total	100	100	100	100

recently published experimental result in obtaining nanopolycrystalline diamond from Karelian shungite by processing in inert refractory ampoules on a spacer under a hydrostatic load of 15 hPa and a temperature of about 1600°C [20]. Apart from nanodiamond clusters with the 15–19 nm size, graphite inclusions or carbon polymorphs with graphite-like structure were also detected in the final product. In view of the conditions of nanodiamond formation from shungite established in this experiment, the authors believe that a scenario of natural diamond formation is quite possible when shungite material is submerged deep in the crust and mantle.

Bearing in mind that in our case we are dealing with explicitly dynamic transformation of shungite not at great depths but in the upper crust, under background conditions not exceeding the level of greenschist facies of metamorphism (see above), we con-

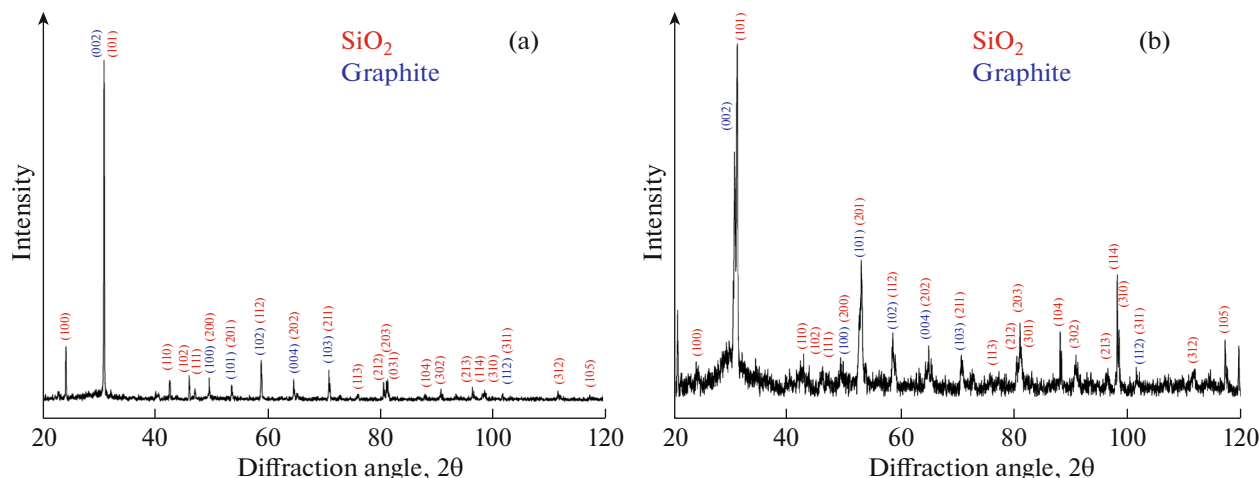


**Fig. 10.** XRD spectra of matrixes of the varieties of SECTION (a) and slickenside (b), suggesting the presence of crystalline phases of quartz and graphite.

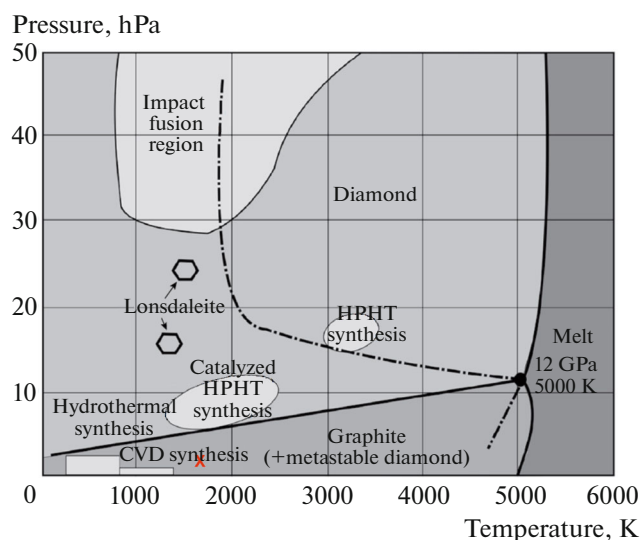


**Fig. 11.** Phase diagram of carbon in  $PT$  coordinates [19] with positions (red index) of diamond and graphite nanoclusters from the slickenside over shungite.

sider that the most realistic scenario was the one realized on a rotary experimental setup at radically low thermodynamic parameters [14]. There, under intense plastic shear of graphite carried out at extremely low pressures of 0.4 and 0.7 hPa, they obtained polymorphs of hexagonal and nanocrystalline cubic diamond, respectively. This allowed the authors of the experiment to conclude that shear plays a generating role in the formation of nanodiamonds at unusually low hydrostatic load. Based on this, and taking into account the specifics of the carbon material transformations described by us under high-speed dynamic displacement, where, judging from the estimates of residual stresses in quartz nanocrystals of upper crustal seismogenic tectonites, pressure could reach 3 hPa [1], and the temperature of frictional heating was in the range of 1450–1650°C [4], we could approximately determine their position in the  $PT$  coordinates of the carbon phase diagram (Fig. 11). We can see here that in our case diamonds fall into the region of metastable growth together with graphite, thus confirming the previously predicted possibility that it can form below the graphite–diamond phase equilibrium boundary [19].

To all of the above, it should be added that the scenario presented here using a natural example of transformation of initially amorphous carbon material into graphite nanoclusters and then into diamond nanoclusters, under conditions of high-speed dynamic shear, in our opinion, confirms and illustrates well the idea that nature-like technologies can be used to create nanodiamond materials important for the industry.

## FUNDING

The work has been carried out as part of the government assignment to the Institute of Physics of the Earth, Institute of Solid State Physics, and Institute of Geology of Ore Deposits, Petrography, Mineralogy, and Geochemistry, Russian Academy of Sciences. The analytical studies have been conducted at the shared laboratory centers of the Institute of Physics of the Earth, Institute of Solid State Physics, Institute of Scientific Information on Social Sciences, and at the IMGRE lab center.

## CONFLICT OF INTEREST

The authors of this work declare that they have no conflict of interest.

## REFERENCES

1. Yu. A. Morozov, A. I. Smul'skaya, A. L. Kulakovskiy, and M. A. Matveev, *Izv., Phys. Solid Earth* **54** (1), 1–22 (2018).
2. Yu. A. Morozov, M. A. Matveev, A. I. Smul'skaya, and A. S. Lar'kov, *Geofiz. Issled.* **25** (4), 5–36 (2024).
3. Yu. A. Morozov, V. S. Sevastianov, A. Yu. Yurchenko, and O. V. Kuznetsova, *Geochem. Int.* **58** (9), 981–994 (2020).
4. Yu. A. Morozov, S. S. Bukalov, and L. A. Leites, *Geofiz. Issled.* **17** (2), 5–18 (2016).
5. A. R. Kotelnikov, G. M. Akhmedzhanova, N. I. Suk, et al., in *Proc. Conf. with International Participation: Shungite Rocks of Karelia: Geology, Structure, Innovation Materials and Technologies "Shungite–2020–2021," Petrozavodsk, June 29–July 1, 2021* (Karelian Sci. Center RAS, Petrozavodsk, 2021), pp. 33–36 [in Russian].
6. M. M. Filippov, Yu. E. Deines, K. I. Lokhov, et al., *Reg. Geol. Metallog.* **67**, 95–106 (2016).

7. V. A. Reznikov and Yu. S. Polekhovskii, *Tech. Phys. Lett.* **26** (8), 689–694 (2000).
8. A. E. Gorshtein, N. Yu. Baron, and M. L. Syrkina, *Izv. Vyssh. Uchebn. Zaved., Khim. Tekhnol.* **22** (6), 711–715 (1979).
9. V. V. Kovalevskii, *Zh. Neorg. Khim.* **39** (1), 31–35 (1994).
10. S. V. Kholodkevich, V. I. Berezkin, and V. Yu. Davydov, *Fiz. Tverd. Tela* **41** (8), 1412–1415 (1999).
11. S. S. Bukalov, L. A. Mikhailitsyn, Ya. V. Zubavichus, L. A. Leites, and Yu. N. Novikov, *Ross. Khim. Zh.* **50** (1), 83–91 (2006).
12. A. C. Ferrari and J. Robertson, *Phil. Trans. R. Soc. London A* **362**, 2477–2512 (2004).
13. M. Hanfland, H. Beister, and K. Syassen, *Phys. Rev. B* **39** (17), 12598–12603 (1989).
14. Y. Gao, Y. Ma, Q. An, et al., *Carbon* **146**, 364–368 (2019).
15. V. D. Blank, B. A. Kulnitskiy, I. A. Perezhogin, et al., *Int. J. Nanotechnol.* **13** (8/9), 604–611 (2016).
16. S. I. Isaenko and T. I. Shumilova, *Uch. Zap. Kazan. Univ., Ser. Estestv. Nauki* **163** (1), 72–87 (2021). <https://doi.org/10.26907/2542-064X.2021.1.72-87>
17. D. Schiferl, M. Nicol, J. M. Zaug, et al., *J. Appl. Phys.* **82**, 3256–3265 (1997).
18. T. Ungar, J. Gubicza, G. Trichy, C. Pantea, and T. W. Zerda, *Compos. A: Appl. Sci. Manuf.* **36**, 431–436 (2005).
19. F. V. Kaminsky and S. A. Voropaev, *Geochem. Int.* **59** (11), 1038–1052 (2021).
20. V. P. Afanas'ev, K. D. Litasov, S. V. Goryainov, and V. V. Kovalevskii, *JETP Lett.* **111** (4), 218–225 (2020).

*Translated by G. Ermakova*

**Publisher's Note.** Pleiades Publishing remains neutral with regard to jurisdictional claims in published maps and institutional affiliations. AI tools may have been used in the translation or editing of this article.